IEEE Access
Multidisciplinary ⋮ Rapid Review ⋮ Open Access Journal

Received May 5, 2021, accepted May 19, 2021, date of publication June 3, 2021, date of current version June 22, 2021.

Digital Object Identifier 10.1109/ACCESS.2021.3086103

Chest X-Ray Outlier Detection Model Using Dimension Reduction and Edge Detection

CHANG-MIN KIM [1], ELLEN J. HONG [2], AND ROY C. PARK [3]
[1]Department of Computer Information Engineering, Sangji University, Wonju 26339, South Korea
[2]Division of Software, Yonsei University, Wonju 26493, South Korea
[3]Department of Information Communication Software Engineering, Sangji University, Wonju 26339, South Korea

Corresponding author: Roy C. Park (roypark1984@gmail.com)

This research was funded by the National Research Foundation of Korea (NRF) Grant funded by the Korea Government (2019R1F1A1060328).

ABSTRACT With the advancement of Artificial Intelligence technology, the development of various applied software and studies are actively conducted on detection, classification, and prediction through interdisciplinary convergence and integration. Among them, medical AI has been drawing huge interest and popularity in Computer-Aided Diagnosis, which collects human body signals to predict abnormal symptoms of health, and diagnoses diseases through medical images such as X-ray and CT. Since X-ray and CT in medicine use high-resolution images, they require high specification equipment and huge energy consumption due to high computation in learning and recognition, incurring huge costs to create an environment for operation. Thus, this paper proposes a chest X-ray outlier detection model using dimension reduction and edge detection to solve these issues. The proposed method scans an X-ray image using a window of a certain size, conducts difference imaging of adjacent segment-images, and extracts the edge information in a binary format through the AND operation. To convert the extracted edge, which is visual information, into a series of lines, it is computed in convolution with the detection filter that has a coefficient of 2^n and the lines are divided into 16 types. By counting the converted data, a one-dimensional 16-size array per one segment-image is produced, and this reduced data is used as an input to the RNN-based learning model. In addition, the study conducted various experiments based on the COVID-chest X-ray dataset to evaluate the performance of the proposed model. According to the experiment results, the LFA-RNN showed the highest accuracy at 97.5% in the learning calculated through learning, followed by CRNN 96.1%, VGG 96.6%, AlexNet 94.1%, Conv1D 79.4%, and DNN 78.9%. In addition, LFA-RNN showed the lowest loss at about 0.0357.

INDEX TERMS Computer-aided diagnosis (CAD) system, feature extraction, line feature analysis (LFA), RNN, deep learning.

I. INTRODUCTION

As the healthcare industry is recently shifting its focus from disease treatment the past to prevention, patients are demanding more effective and safe treatment and personalized treatment from medical care providers [1]–[3]. To achieve this, it is necessary to comprehensively analyze and utilize patients' lifelong data, medical image data, genetic data, medical literature data, and medical records in hospitals. There are limitations in diagnosing patients by analyzing the vast amounts of data through doctors' cognitive judgment ability and effort, and environmental factors [4]–[7]. Thus, studies have been actively conducted on AI technologies that assist and replace doctors to analyze patients' data and support decision-making. Even for the same disease, doctors have huge differences in treatment and lack consistency [8]–[10]. Since healthcare determines a person's life and diagnoses diseases, its diagnosis accuracy is very important. Patients' confidence is increasing toward AI-based healthcare technology with fast computational power and high accuracy based on diagnosis evidence [11]–[15]. Medical imaging technology in AI is one of the fields with the most active

The associate editor coordinating the review of this manuscript and approving it for publication was Sudhakar Radhakrishnan.

research. To diagnose a disease, medical images collect various parts inside and outside the human body through an image collecting device, and clinical or image medical specialists use the collected images for diagnosis by relying entirely on their visual cognitive ability and judgment. However, such an existing method is being improved or replaced by AI [16]–[18]. Many studies are actively in progress because AI can recognize the characteristics of image data more accurately and faster than doctors. In particular, the recent outbreak of an unprecedented COVID-19 pandemic has increased the interest in responding to diseases by using new technologies such as AI and data to detect chest diseases, leading to more active related studies [19]–[25].

Huang [26] proposes a system that uses a 3D Convolutional Neural Network (CNN) from CT data to detect lung nodules. It uses the prior knowledge of lung nodules, confusing anatomical structures, data-based machine learning functions, and classifiers. The CNN especially reduces structure variability further by producing nodule candidates using a topical geometric model-based filter and assuming the topical direction. Zhu [27] proposes Deep Lung to detect two components of nodule detection and classification, for which two deep 3D DPNs are designed, respectively, given the 3D characteristics of lung CT data and the compressibility of DPN (Double Path Network). To effectively learn the features of a nodule, 3D Faster Regions with R-CNN (Convolutional Neural Net) are designed to detect nodules using an encoder-decoder structure such as a 3D Double Path Block and U-net. Bhandary [28] proposes a modified AlexNet (MAN) to detect lung abnormalities, with a deep learning framework to predict lung cancer and pneumonia. He initially uses modified AlexNet for chest X-ray diagnosis and implements SVM for classification in the modified AlexNet.

Despite many studies, disease diagnosis systems based on medical images require several calculations and longer time for an AL model to learn and recognize high-quality medical images, reducing the speed of software development and research [29]. Although hardware devices are generally replaced by high-performing ones to increase speed, this also leads to new problems since high-performance equipment and high-quality networks incur huge costs in creating an AI environment and consume a huge amount of energy. It is also difficult to create an AI environment in small mobile devices, which also have the issues of heating and battery discharge due to limited resources [30]–[34].

To solve these problems, this study will propose a Chest X-ray outlier detection model using dimension reduction and edge detection. The proposed method will accurately identify the disease using the X-ray of 'chest disease patients.' The large size of the input image data lowers the processing speed and may impede accurate analysis due to the restrictions on resource use. To overcome this, the study proposed a Line-Feature Analysis algorithm that converts high-quality, high-resolution original images into low-dimension data to reduce the data processing speed for accurate analysis. For the accuracy and reliability of the LFA algorithm proposed in this study, accuracy was measured in an experiment according to the edge detection algorithm, and the performance of the LFA-RNN model was compared with the existing learning model to confirm its performance. This paper is structured as follows. Chapter 2 describes an AI-based precise chest disease diagnosis service and the dimension reduction technology of medical images. Chapter 3 shows the data production through the dimension reduction LFA technique proposed in this paper, the RNN model designed to learn LFA data, and the chest X-ray outlier detection-based chest disease detection system based on it. Chapter 4 tests the performance of the proposed algorithm through an experiment, and Chapter 5 is the conclusion of this study.

II. RELATED RESEARCH

A. AI-BASED PRECISE CHEST DISEASE DIAGNOSIS SERVICE

As a very serious health problem in people's everyday lives, chest diseases include chronic obstructive lung disease, pneumonia, asthma, tuberculosis, and lung disease. Since professionally trained physicians are needed to detect chest disease, studies on chest disease diagnosis using AI methodology are actively in progress these days. Korean company VUNO [35] developed VUNO-med, a CT image-based lung nodule detection AI software solution that learns, diagnoses, and assists AI-based medical data. VUNO-med is a diagnosis and assistive technology that has doctor-level accuracy by extracting the features of CT images on lung disease and lung cancer. The model learns X-ray image data and automatically reads pediatric bones age through deep learning, which is an AI technology, presenting the bone age as a probability with an accuracy of 96% or higher. The technology learns a lung image based on the lung CT image and reads the parts that are difficult for medical specialists to read, which has 97% of accuracy, searches similar patients based on this, and assists with the diagnosis.

Figure 1 shows auto lung nodule detection software of Samsung Electronics. To detect chest diseases, Samsung Electronics has developed Auto Lung Nodule Detection (ALND), which is AI-based diagnosis assistive software [36] that assists a doctor in diagnosis by marking the area of suspected lung nodule on the chest PA X-ray image.

This technology has applied Samsung's own deep learning technology and has already completed clinical tests in multiple domestic and overseas hospitals, with approval at more than 80% of sensitivity and 0.15 false-positive cultures per image. It also provides an option (Autorun) that automatically performs ALND immediately after chest X-ray shooting depending on the user's workflow, and it provides flexibility through three options of transmitting to PACS according to the hospital environment. Several calculations and much time are required for the AI model to learn and recognize high-quality medical images in a diagnosis system. Thus, a study on dimension reduction is needed to convert high-dimension data into low-dimension and use them in learning and recognition by the AI-model.

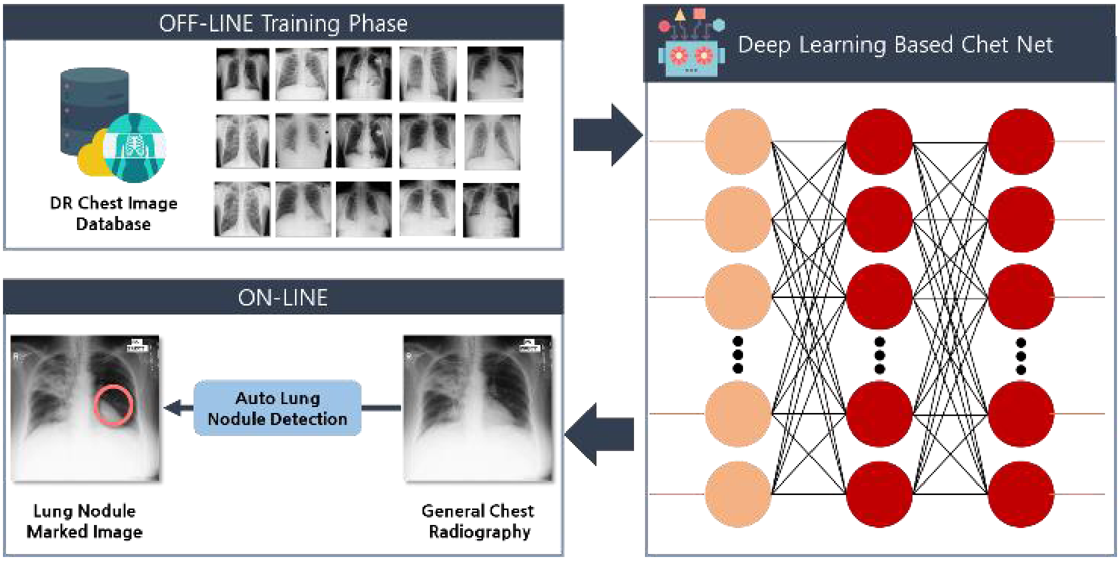

FIGURE 1. Auto lung nodule detection software of Samsung electronics.

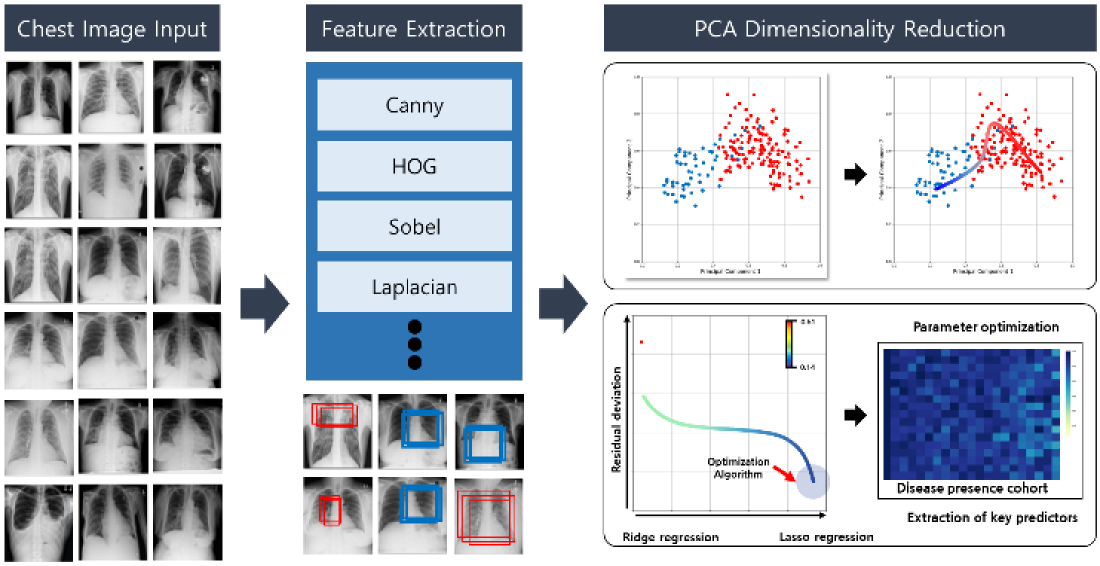

FIGURE 2. Dimensionality reduction process of PCA.

B. MEDICAL IMAGE DIMENSION REDUCTION TECHNOLOGY

The medical image dimension reduction technologies used for medical devices to smoothly read data include Linear Discriminant Analysis (LDA), Independent Component Analysis (ICA), and Principal Component Analysis (PCA). ICA separates independent signals mixed with each other, and the greater the amount of data is, the closer the distribution becomes to the Gauss function [37]. Next, PCA converts high-dimension space to low-dimension without linear association by finding new axes orthogonal to each other while preserving the dispersion of data as much as possible. Figure 2 shows the dimensionality reduction process of PCA, which produces new features by linearly combining all features of the data. It converts the input data into a covariance matrix during the combination and defines the eigenvector as the principal component by $\sum$ the unknown dimension coefficient vector in this matrix. However, it is difficult to identify which class is used by PCA to calculate since it projects high-dimension into low-dimension using a variance, and the number of main components changes according to the input data. That is, if the learning and test data do not apply PCA at the same time, a classifier cannot be used due to the different size of the principal components derived from the two data, but performing PCA at the same time makes the application on real-life data difficult. In addition, the number

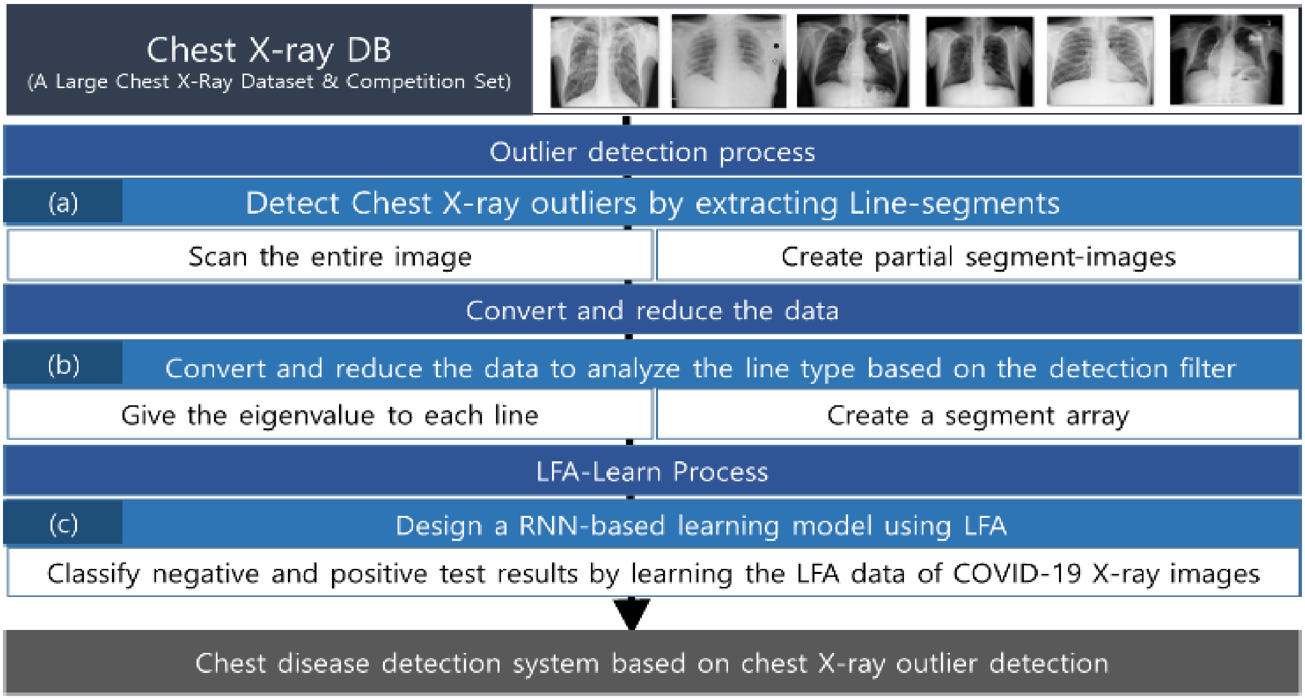

FIGURE 3. Processing of chest X-ray outlier detection model using dimension reduction and edge detection.

of main components changes as the classification criteria changes according to the number of learning data, and such criteria must be re-established by combining with the original data even if additional data are collected [38].

This study complements these shortcomings and proposes an algorithm that easily interprets the reduced data by reducing the size of data while keeping all line characteristics of the X-ray image as much as possible. It maintains the unique shape of each object and collects the characteristics of weak and strong lines that have their own shape by aggregating the lines. A rough classification criterion is formed based on the strong line in the class, and the model is designed to classify objects in more detail based on the weak characteristics. In addition, the proposed algorithm is easy to apply since it does not change the size of result data according to the data characteristics such as PCA and calculates data of a certain size, so only additional data can be used as learning data immediately after processing.

III. CHEST X-RAY OUTLIER DETECTION MODEL USING DIMENSION REDUCTION AND EDGE DETECTION

Existing medical image-based diagnosis systems require several calculations and a longer time for an AI model to learn and recognize high-quality medical images. Another problem is that accurate diagnosis cannot be made since high-quality images lower the speed of software development and research. Thus, this paper proposes a chest X-ray outlier detection model using dimension reduction and edge detection to solve this problem. It presents a line-segment feature analysis algorithm to extract the characteristics from chest X-ray images taken by the system to diagnose a chest disease as well as an RNN structure to construct a model that can recognize an image segmentation-based chest disease.

Figure 3 shows the processing of the chest X-ray outlier detection model using dimensionality reduction and edge detection, which is divided into outlier detection, data conversion and reduction, and a learning process.

A. CHEST X-RAY OUTLIER DETECTION THROUGH LINE-SEGMENT EXTRACTION

COVID-19 frequently has cardio-vasal shadow within limits on the X-ray and becomes similar to pneumonia as the left basilar becomes larger and opaque. It also shows symptoms such as progressive infiltrate and consolidation, small consolidation in the right upper lobe, and ground-glass opacities [39], [40]. To comprehend such symptoms, the entire area of the image is scanned through a same-size window, which produces partial segment-images by scanning X-ray images at regular intervals. For the produced images, the difference-of-images technique is applied to separate the foreground area from a computer vision by using three adjacent segment-images, which are overlapped with each other to use the partial foreground images. This is possible in high-resolution images since the higher number of pixels in the image enables the window to move closer and obtain a sufficient foreground. Figure 4 represents the segment-image detection process. Algorithm 1 shows the operation process of figure 4.

Figure 4 shows the segment-images (C1, C2, and C3) extracted by scanning an X-ray image through a window of M×N size and a binary image detected by intersecting the

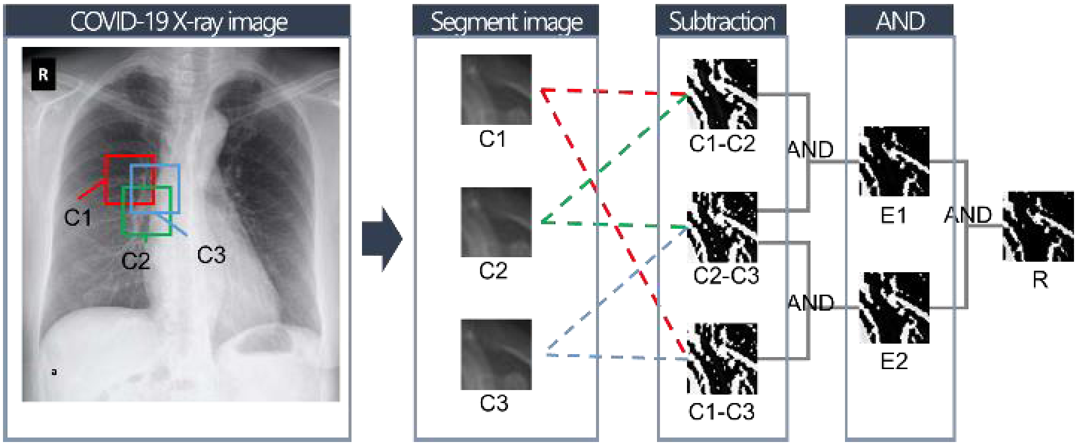

FIGURE 4. Three adjacent segment-image sets detected through windows.

Algorithm 1 Edge Detection for Segment-Image

// X: X-ray image, M, N : *size of window*
Input: *X, M, N*
def *threshold*($I1$, $I2$):
  $I1I2_{sub} = I1 - I2$
  // OTSU: Otsu Algorithm, Thresholding
  return $\begin{cases} 255, & I1I2_{sub} > \text{OTSU}(I1I2_{sub}) \\ 0, & I1I2_{sub} \leq \text{OTSU}(I1I2_{sub}) \end{cases}$
def *edge detection for segment-image*:
  // segmented image : sImg
  $sImg = [][]$
  $W, H = X.shape$
  for w ***from*** *0* ***to*** *W-M*:
    for h ***from*** *0* ***to*** *H-N*:
      $sImg[w, h] = \text{X}(w + M, h + N)$
  $R = []$, $No = 0$
  for *j* ***from*** 0 ***to*** *W-M-1* ***do***:
    for *i* ***from*** *0* ***to*** *H-N-*1 ***do***:
      $C1, C2, C3 = sImg[i,j], sImg[i,j+1], sImg[i+1,j]$
      // threshold function
      $C1C2 = threshold(C1, C2)$
      $C2C3 = threshold(C2, C3)$
      $C1C3 = threshold(C1, C3)$
      // AND operation
      $E1 = C1C2 \wedge C2C3$
      $E2 = C2C3 \wedge C1C3$
      $R[No{+}{+}] = E1 \wedge E2$
Output: *R*

extracted images and by applying subtraction and AND operation. As shown in Figure 4, segment-images are adjacent to each other in a certain direction, which is grouped into (C1, C2), (C2, C3), and (C1, C3) to apply the difference image technique (subtraction). The difference image technique was designed to accurately extract the object appearing through the foreground image prepared in advance by pre-taking the foreground of the space where the object will be located. To compensate for having to prepare the foreground image in advance, the object is extracted through multiple images with temporal differences. By applying this method to high-resolution images, the edge of an object is extracted through minute pixel differences, and the AND operation is performed by crossing the results of the extracted images. The AND operation eliminates the noise that could not be removed in the segment-image process and highlights the characteristics of the extracted line more clearly. In Figure 4, the images detected through the subtraction operation are E1 and E2, and the final image derived through the AND operation is shown as the edge for C2 located in the middle among the three adjacent segment-images. The data calculated through this process shows a binary format with line characteristics for some of the X-ray images. This visual line data is converted into a series of number patterns to be computed and used easily.

B. DATA CONVERSION AND REDUCTION FOR DECTION FILTER-BASED LINE-TYPE ANALYSIS

The previous step applied the difference image technique by crossing adjacent segment-images with each other, and extracted binary data for the edge was extracted through AND operation. However, it is difficult to identify the type of the same line since this data is visual information. It could be identified by converting the line type of the object existing in the image into a series of number patterns using the detection filter. Figure 5 shows the standardization conversion of visual data patterns using the filter. The information of line-line type is calculated by convoluting each segment-image extracted from Section 3.1 to a 2×2 detection filter $(*)$ with a coefficient of 2^n. This operation gives an eigenvalue to the line in each of the segment-images, which are as in Table 1. Table 1 shows the information of line type that can be identified through the 2×2 detection filter, which changes visual images into number patterns and is the same

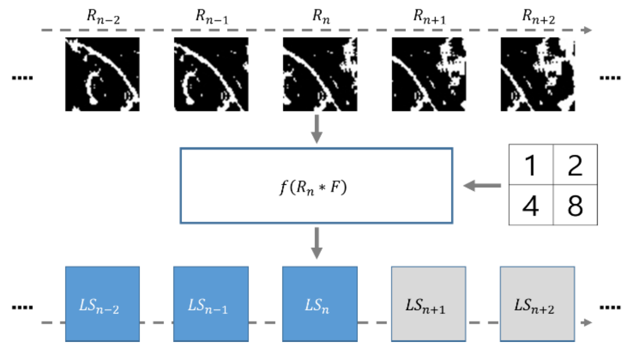

FIGURE 5. Standardization conversion of visual data patterns using detection filter.

TABLE 1. The eigenvalue for each line type.

Pattern	Line Type	Pattern	Line Type
0000 (0)	Non-Activity	8000 (8)	Point
0001 (1)	Point	8001 (9)	Verticality
0020 (2)	Point	8020 (10)	Diagonal
0021 (3)	Horizontality	8021 (11)	Curve
0400 (4)	Point	8400 (12)	Horizontality
0401 (5)	Diagonal	8401 (13)	Curve
0420 (6)	Verticality	8420 (14)	Curve
0421 (7)	Curve	8421 (15)	Activity

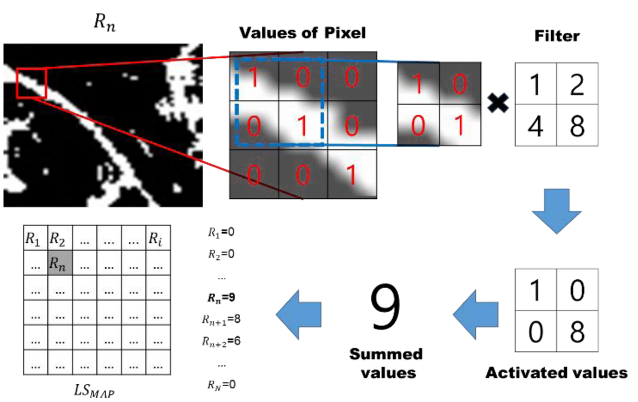

FIGURE 6. Visual image compression using a convolution-based detection filter.

as converting binary numbers into decimal numbers in the engineering field. All objects have their own unique shape, which is used as one of the key characteristics to classify data. A detection filter was applied to extract such characteristics effectively, and binary edge detection was performed to use the filter. Figure 6 shows a visual image compression using a convolution-based detection filter and how the detection filter and segment-image are convoluted. As shown in Figure 6, R means binary edge data and scans all pixels by performing multiplication with the same size as the detection filter.

Algorithm 2 Visual Image Compression

```
// X: segmented image, W, H : size of window
Input: X[x0, x1, x2, ..., xN], W, H

def visual image compression:
  // lien segment map : LS_MAP
  LS_MAP = [][]
  Filter = [[1, 2], [3, 4]]
  // Fs is the filter size.
  Fs = len(Filter)/2

  for x from X do
    for w from 0 to W-Fs do
      for h from 0 to H-Fs do
        r = X(w:w+Fs, h:h+Fs)*Filter
        LS_MAP[w][h] = sum_ft(r)

Output: LS_MAP
```

Each of the response coefficients is generated according to the edge detection result, which is summed and expressed as one eigenvalue. An LS_{map} with the value as the coefficient is produced. The converted data is expressed as one of the numbers from 0 to 15, as shown in Table 1, and the line type can be identified. Using the LS_{map} calculated, each of the segment-images is converted into 16-size 1D data. Equation 1 shows the production process of the 1D array using LS_{map}.

Algorithm 2 shows the pseudo code for figure 6.

$$\begin{aligned} &LFA_n = 0_i, 0 \in Z^I \\ &\text{where, } LFA_n[LS_{map}(x, y)] \\ &\quad = LFA_n[LS_{map}(x, y)]+1; \\ &\quad\quad \mathit{while}\ (0 \le x < W \text{ and } 0 \le y < H) \end{aligned} \tag{1}$$

W and H in Formula 1 indicate the size of LS_{map}, and LFA_n is the 1D array to aggregate the line type on the nth segment-image. I shows the number of line segment types, meaning 16. A range from 0 to 15 can be used if each coefficient value of LS_{map} is extracted and used as the index of LFA_n. Since the coefficient value means the eigenvalue of line type, the value of the array increases by one if the array index is called to count the number of lines. The 1D array has values for 16 line-types in total, and a final matrix of the "number of segment-images" $\times$ 16 sizes is produced from the X-ray image. The data is reduced based on the line of objects through this process.

C. CONFIGURATION AND PROCESSING OF CHEST DISEASE DETECTION SYSTEM

Based on the above experiment results, this study developed a chest disease detection system based on Chest X-ray outlier detection, which takes CT and X-ray images of lung disease patients and sends them to the server to analyze the data and

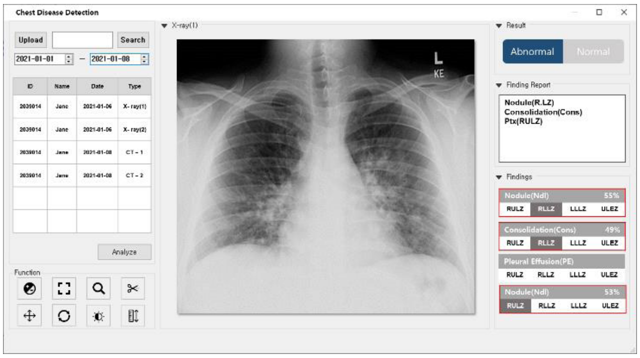

FIGURE 7. Chest disease detection system based on chest X-ray outlier detection.

predict disease. To predict the disease accurately, the system rotates the images automatically rotated to the correct position and checks if all patients' lung areas are covered. This Chest X-ray outlier detection system is very effective since it provides basic information to medical doctors with insufficient diagnosis experience and supports their decision-making by lowering the false diagnosis rate and enabling accurate diagnosis. Figure 7 shows the chest disease detection system based on the Chest X-ray outlier detection. The implemented system can analyze data and predict diseases as it receives patients' chest X-ray images and obtains information on the images uploaded with a user ID, name, and date set as search conditions. The system receives user X-rays as the input and analyzes data by expanding, reducing, moving, and contrasting the data. It also provides information on the overall lung structure and provides information about the disease the user has by designating the X-ray. It can detect 15 diseases, which can be identified through probability.

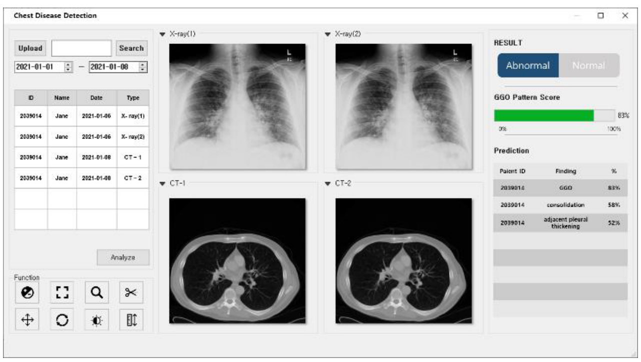

FIGURE 8. Chest X-ray outlier detection-based chest disease detection screen.

Figure 8 shows the chest disease detection screen based on Chest X-ray outlier detection. The X-rays show a PA (Posterior to Anterior) view and can distinguish PA and AP views and the rotated chest PA. Since the opacity of Chest X-rays increases when lung disease occurs, pulmonary opacification is used to determine and identify a lung disease, especially through the opacity degree of the air layer. This judged by Ground-Glass Opacifications (GGO), Consolidation, and Ateletasis patterns. The GGO pattern can confirm both blood vessels and air layers through X-rays for results. Consolidation is used when blood vessels are completely invisible, and Ateletasis is used when blood vessels contract and become difficult to distinguish. GGO is the main pattern for COVID-19 patients, showing the inner structure with blurred opacity. Pneumonia symptoms were usually suspected through the x-ray at first, but it is often normal.

Thus, it is difficult to determine early or mild COVID-19 patients through X-rays. Since only severe COVID-19 cases can be detected through X-rays, it is too late to treat patients. GGO-based Chest CT is used to solve this. As seen in the figure, the X-ray showed no symptoms of COVID-19 but later showed blurry opacity on the left side, and a GGO pattern clearly showing blood vessels appeared in the CT result. In addition, Consolidation occurred when the GGO pattern became severe or turned white, with various cases such as Lobar, focal consolidation, ill-defined consolidation, white-out, and multifocal ill-defined consolidation. Among them, multifocal ill-defined consolidation indicates the most common symptoms in COVID-19 patients, 83% of whom had GGO patterns, and 58% had Consolidation at the same time. Also, adjacent pleural thickening, interlobular septal thickening, and air bronchograms were 52%, 48%, and 46%, respectively, in the patients.

TABLE 2. Structure of proposed-RNN.

No.	Layer Name
1	Input Layer (*N*)
2	Convolution (64, *N*, std=1, pad="same," act="relu")
3	BatchNormalization
4	Reshape (64, N)
5	Bidirectional-GRU (64)
6	Bidirectional- GRU (32)
7	Dropout (0.2)
8	Output Dense Layer (act="sigmoid")

IV. PERFORMANCE EVALUATION

In this chapter, an RNN-based learning model is designed using LFA, and its performance is evaluated. The proposed structure is a model to learn dimension reduction data produced through an LFA algorithm and has a total of 8 layers, including input and output layers. Table 2 shows the RNN structure proposed in this study. N in the Input layer represents the size of input data. It is used as a preprocessing concept to reinforce features through a one convolution layer and prevents overfitting in the learning process with a "Batch-Normalizaton" layer. To use the circulation layer, the size of the input data is redefined through the "Reshape layer," and the dimension reduction data calculated through each segment-image is input through two Bidirectional-GRUs.

Classification patterns are identified among the data continuously input through the two circulation layers, which has 64 and 32 units each. After the circulation layer, the model passes the "Dropout" layer and the Dense and finally output the results. The data with the reduced images of COVID-19 X-ray are learned through this learning model to classify negative and positive results. LFA-RNN model recorded the weight of the lowest loss among numerous epochs measured in ModelCheckpoint(), and lowered the learning rate of optimizer when no loss was changed during a certain period of time by using ReduceLROnPlateau(). As the optimizer of the model, RMSprop was used.

The experiment was composed of two parts to measure the accuracy and reliability of the algorithm proposed in this study. The first part measures accuracy by comparing the algorithm of proposed edge detection with the algorithms of Laplacian, Sobel, and Canny edge detections, which are widely known.

Second, the study compared the performance of the proposed learning model with CRNN, AlexNet VGG, Conv1D, and DNN, which are the existing learning models. The performance was evaluated on Windows 10 64-bit, Intel Core i7-7700K CPU, 32GB RAM, and NVIDIA GeForce RTX 3090.

A. ACCURACY CHANGES OF THE LFA-RNN MODEL ACCORDING TO THE EDGE DETECTION ALGORITHM

This section conducted an experiment to measure the accuracy of the edge detection of the proposed LFA algorithm. Its performance was compared with that of Laplacian, Sobel, and Canny, which are well-known edge detection algorithms. Various parameters were applied in advance to the existing edge detection algorithms to conduct the experiment, and the value with the highest accuracy was set as the parameter value. For an accurate experiment, the COVID-19 chest X-ray dataset [34] was used, and 80% of the database was classified as learning data and 20% as test data. Figure 9 shows the accuracy measurement result of the edge detection algorithm.

Figure 9 (a) is the accurate measurement result, and (b) is the loss for each algorithm. The proposed algorithm shows the highest accuracy at 98.9%, followed by Canny (97.9%), Sobel (97.6%), and Laplacian (98.2%). These results are closely related to the edge detection results as the proposed dimension reduction algorithm produces a new feature map using the lines. That is, when the edge detection algorithm is highly similar to the original data, the learning model through the proposed dimension reduction technique also shows high accuracy. Figure 9 (b) shows the results of measuring the loss, and the proposed algorithm has the lowest loss at 0.067, followed by Sobel 0.113, Canny 0.124, and Laplacian 0.215. This confirms that the proposed algorithm has the best edge detection performance. In addition, the three algorithms compared during the edge detection experiment set the parameter that had the best result from the combination of various parameters in the prior experiment. On the contrary, since the proposed algorithm can be used without setting a parameter value since thresholds are calculated internally during

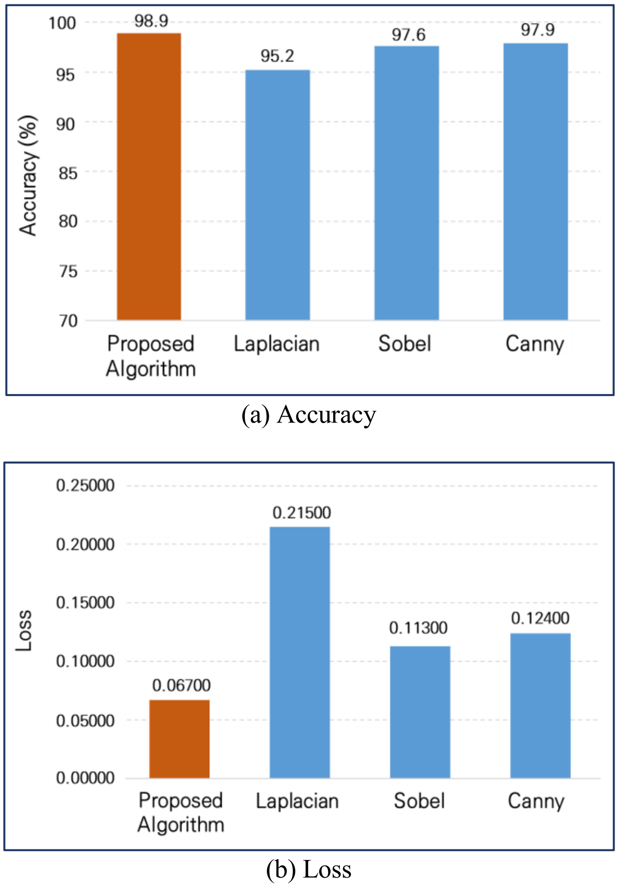

FIGURE 9. Results of measuring accuracy according to the edge detection algorithm.

the edge detection, it is considered more effective than the existing algorithm.

Laplacian edge algorithm offers the edge judgment point (zero crossing) through quadratic differential so that it is able to detect detailed edges. Therefore, edges in all directions are detected. Nevertheless, the algorithm is very sensitive to noise. Accordingly, the noise of brightness occurs in all regions and causes inaccurate detection of regions. As a result, it is judged to influence negatively accuracy of LFA-RNN. Although Sobel edge algorithm is effective for emphasizing the central value of an input image and for averaging a saliency value, it responds more sensitively to the edge in a diagonal direction. In case of X-ray image data only with brightness, their background and internal regions are separated extremely, so it is possible to detect the edge of an outer region effectively. Nevertheless, it has low performance in detecting detailed edges. For this reason, accuracy of LFA-RNN is judged to be lowered. Canny edge algorithm shows strong performance in terms of a low error rate, high accuracy, and single point matching, but has several problems. Due to its complicated implementation and long execution time, it is inappropriate for real-time image processing. Since it is also applied equally to the gradient processed with a threshold, it shows sensitive performance difference in thresholds. In X-ray images, brightness of bones is similar to

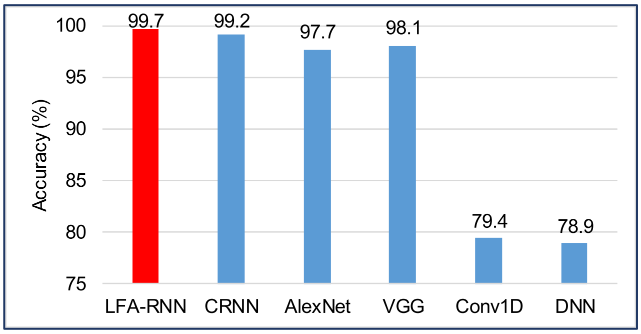

(a) Accuracy

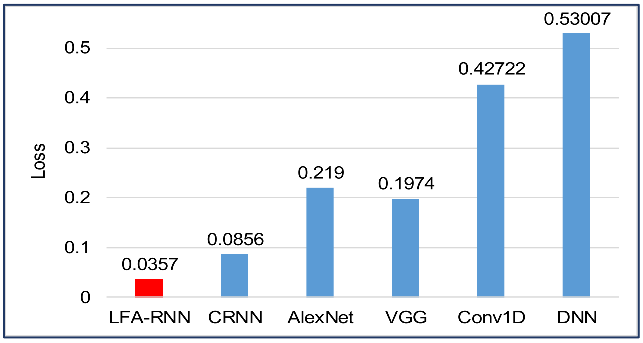

(b) Loss

FIGURE 10. **Results of accuracy and loss measurement.**

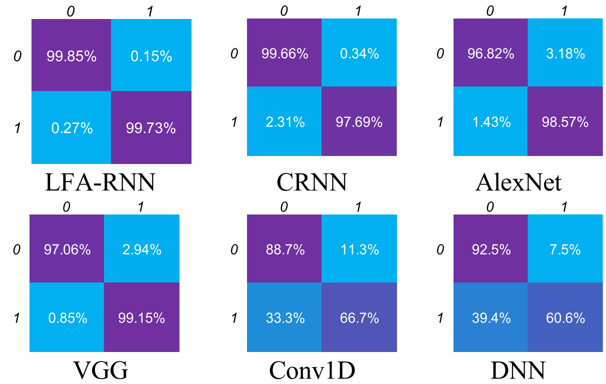

(a) Confusion-Matrix

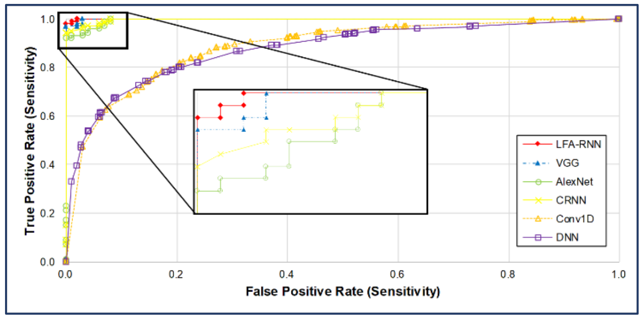

(b) ROC curve of each algorithm

FIGURE 11. **Results of confusion-matrix and ROC curve evaluation for each algorithm.**

that of skin. For this reason, it is hard to set up an appropriate threshold for the classification, and it is possible to draw inaccurate contour information due to the fine brightness of each image. As a result, accuracy of LFA-RNN model is judged to be lowered somewhat.

The contour detection method introduced in the thesis splits an X-ray image by a certain size first and then applies the technique of Fig. 4 to each split region, so it is possible to minimize brightness noise in the image and detect an edge. Additionally, since the split regions seem to be overlaid, it is possible to prevent regions from being detected due to brightness noise in adjacent split regions. In this way, the method is capable of extracting detailed edges effectively. Therefore, the proposed algorithm is judged to have higher accuracy than other algorithms in comparison.

B. ACCURACY CHANGES OF THE LFA-RNN MODEL ACCORDING TO THE EDGE DETECTION ALGORITHM

An experiment was conducted using CRNN, AlexNet, VGG, Conv1D and DNN as comparison models to evaluate the performance of the proposed RNN model, and the learning data was gradually reduced to compare the accuracy for verifying its learning ability. There was a total of 950 datasets (normal image: 482, COVID-19 image: 468), with 70% learning data (665), 10% verification data, 10% (95), and 20% test data (190). Figure 10 shows the results of measuring accuracy and loss. The accuracy of the proposed LFA-RNN model shows the highest accuracy at 99.7%, and the loss shows the lowest value at 0.0357. Its performance was strong in the order of CRNN (99.2%), VGG (98.1%), AlexNet (99.7%), Conv1D (79.4%) and DNN (78.9%).

Next, the study measured Confusion-Matrix, and the Receiver Operating Characteristic (ROC) curves for the accuracy and reliability of the proposed algorithm, which are shown in Figure 11. The result of measuring Confusion-Matrix represents the ratio of the samples that are TRUE among the samples predicted to be true by each class for the chest disease. For an average confusion-matrix, LFA-RNN showed 99.7%, CRNN 98.6%, AlexNet 97.7%, and VGG 98.1%, Conv1D 77.7%, DNN 76.5%, which were better results than the comparison model in all classes. Each class can clearly extract the data for a better precision result because the LFA technique compresses the original images to produce new data and reduces the data size by using only some strong features and removing detailed features. In all the experiments, the proposed LFA-RNN model showed a stable graph in learning and verification and the highest performance at 99.7% in the evaluation using test data. It also showed the lowest loss at about 0.0357 and the highest performance results in precision and recall tests.

V. CONCLUSION

This paper proposes a chest X-ray outlier detection model using dimension reduction and edge detection. Unlike the existing dimension reduction techniques, the proposed algorithm uses its own data as the standard for dimension reduction and always applies a consistent classification criterion.

In the existing techniques, classification criteria changed according to the number of learning data, class distribution, and type. However, this may degrade the performance of recognition by reanalyzing the classification criteria and using inefficient classification when applied to additional learning data and daily life data. The algorithm proposed by this paper uses only images to reduce the dimension by preserving their own features as much as possible. Dimension was reduced around the appearance of objects when classifying them, and the edge detection technique is preceded to obtain the object's appearance information. Edge detection produces three different images by extracting and crossing three segment-images adjacent to each other on a window of a certain size. After conducting AND operation on the produced images, binary edge information is extracted by removing the noise that could not be removed by the difference image. The extracted edge information shows an edge through visual information, which is converted into a number pattern through a 2×2 detection filter and added to produce an eigenvalue for the type of line. The eigenvalue can show a total of 16-line types, which are counted to produce 16-size 1D data. This data can certainly reduce the original image by segmenting the X-ray image by three and producing 1D data, and it can maintain the shape of each object as much as possible since the reduction method is aggregated around the unique shape of the object. Such produced data is used as an input of the RNN-based learning model, and the reduction data of each segment in a circulation layer is inputted to detect anomalies in the entire X-ray image to determine whether the X-ray image of COVID-19 is positive or negative. The proposed method classifies the line features of the learning input pattern based on the medical image and creates a new feature through the aggregation, enabling clearer dimension reduction criteria as well as constant size and aggregation.

At present, LF algorithm reduces an image size on the basis of a contour line. For medical diagnosis, a color is also used as critical diagnosis information. In the future, we will additionally research a color region in LFA algorithm, and thereby try to develop a more effective diagnosis system.

REFERENCES

[1] C.-M. Kim, R. C. Park, and E. J. Hong, "Breast mass classification using eLFA algorithm based on CRNN deep learning model," *IEEE Access*, vol. 8, pp. 197312–197323, Oct. 2020.

[2] D.-H. Shin, R. C. Park, and K. Chung, "Decision boundary-based anomaly detection model using improved AnoGAN from ECG data," *IEEE Access*, vol. 8, pp. 108664–108674, Jun. 2020.

[3] M. Mahmud, M. S. Kaiser, and A. Hussain, "Deep learning in mining biological data," *Cogn. Comput.*, vol. 13, no. 1, pp. 1–33, Jan. 2021.

[4] Y. Gao, D. Lu, G. Li, G. Wang, Q. Chen, L. Liu, and D. Li, "Comparative analysis of modeling algorithms for forest aboveground biomass estimation in a subtropical region," *Remote Sens.*, vol. 10, no. 4, pp. 627–648, Apr. 2018.

[5] M. M. Li, S. Sengupta, and M. D. Hanigan, "Using artificial neural networks to predict pH, ammonia, and volatile fatty acid concentrations in the rumen," *J. Dairy Sci.*, vol. 102, no. 10, pp. 8850–8861, Oct. 2019.

[6] S. Wu, S. Zhong, and Y. Liu, "Deep residual learning for image steganalysis," *Multimedia Tools Appl.*, vol. 77, no. 9, pp. 10437–10453, Feb. 2017.

[7] A. K. Singh, A. Kumar, M. Mahmud, M. S. Kaiser, and A. Kishore, "COVID-19 infection detection from chest X-ray images using hybrid social group optimization and support vector classifier," *Cognit. Comput.*, Mar. 2021, doi: 10.1007/s12559-021-09848-3.

[8] H. Yoo, S. Y. Han, and K. Y. Chung, "A frequency pattern mining model based on deep neural network for real-time classification of heart conditions," *Healthcare*, vol. 8, no. 3, pp. 234–252, Jul. 2020.

[9] J.-W. Baek and K. Chung, "Context deep neural network model for predicting depression risk using multiple regression," *IEEE Access*, vol. 8, pp. 18171–18181, Jan. 2020.

[10] V. N. M. Aradhya, M. Mahmud, D. S. Guru, B. Agarwal, and M. S. Kaiser, "One-shot cluster-based approach for the detection of COVID-19 from chest X-ray images," *Cognit. Comput.*, Mar. 2021, doi: 10.1007/s12559-020-09774-w.

[11] J.-C. Kim and K. Chung, "Multi-modal stacked denoising autoencoder for handling missing data in healthcare big data," *IEEE Access*, vol. 8, pp. 104933–104943, May 2020.

[12] J.-C. Kim and K. Chung, "Hybrid multi-modal deep learning using collaborative concat layer in health bigdata," *IEEE Access*, vol. 8, pp. 192469–192480, Oct. 2020.

[13] K. Chung and H. Jung, "Knowledge-based dynamic cluster model for healthcare management using a convolutional neural network," *Inf. Technol. Manage.*, vol. 21, no. 1, pp. 41–50, Aug. 2019.

[14] B. Barile, A. Marzullo, C. Stamile, F. Durand-Dubief, and D. Sappey-Marinier, "Data augmentation using generative adversarial neural networks on brain structural connectivity in multiple sclerosis," *Comput. Methods Programs Biomed.*, vol. 206, Jul. 2021, Art. no. 106113, doi: 10.1016/j.cmpb.2021.106113.

[15] D. Karimi, S. K. Warfield, and A. Gholipour, "Transfer learning in medical image segmentation: New insights from analysis of the dynamics of model parameters and learned representations," *Artif. Intell. Med.*, vol. 116, Jun. 2021, Art. no. 102078, doi: 10.1016/j.artmed.2021.102078.

[16] Y. Li, J. Wu, and Q. Wu, "Classification of breast cancer histology images using multi-size and discriminative patches based on deep learning," *IEEE Access*, vol. 7, pp. 21400–21408, Feb. 2019.

[17] L. Sun, J. Wang, Z. Hu, Y. Xu, and Z. Cui, "Multi-view convolutional neural networks for mammographic image classification," *IEEE Access*, vol. 7, pp. 126273–126282, Sep. 2019.

[18] K. Chung, H. Yoo, and D.-E. Choe, "Ambient context-based modeling for health risk assessment using deep neural network," *J. Ambient Intell. Humanized Comput.*, vol. 11, no. 4, pp. 1387–1395, Apr. 2020.

[19] K. Chung and R. Park, "P2P-based open health cloud for medicine management," *Peer-Peer Netw. Appl.*, vol. 13, no. 2, pp. 610–622, Aug. 2019.

[20] A. Afifi, N. E. Hafsa, M. A. S. Ali, A. Alhumam, and S. Alsalman, "An ensemble of global and local-attention based convolutional neural networks for COVID-19 diagnosis on chest X-ray images," *Symmetry*, vol. 13, no. 1, pp. 113–137, Jan. 2021.

[21] J. E. Luján-García, M. A. Moreno-Ibarra, Y. Villuendas-Rey, and C. Yáñez-Márquez, "Fast COVID-19 and pneumonia classification using chest X-ray images," *Mathematics*, vol. 8, no. 9, pp. 1423–1441, Aug. 2020.

[22] S. Lalmuanawma, J. Hussain, and L. Chhakchhuak, "Applications of machine learning and artificial intelligence for COVID-19 (SARS-CoV-2) pandemic: A review," *Chaos, Solitons Fractals*, vol. 139, Oct. 2020, Art. no. 110059, doi: 10.1016/j.chaos.2020.110059.

[23] T. K. Dash, S. Mishra, G. Panda, and S. C. Satapathy, "Detection of COVID-19 from speech signal using bio-inspired based cepstral features," *Pattern Recognit.*, vol. 117, Sep. 2021, Art. no. 107999, doi: 10.1016/j.patcog.2021.107999.

[24] M. C. Younis, "Evaluation of deep learning approaches for identification of different corona-virus species and time series prediction," *Comput. Med. Imag. Graph.*, vol. 90, Jun. 2021, Art. no. 101921, doi: 10.1016/j.compmedimag.2021.101921.

[25] O. P. Idowu, A. E. Ilesanmi, X. Li, O. W. Samuel, P. Fang, and G. Li, "An integrated deep learning model for motor intention recognition of multi-class EEG signals in upper limb amputees," *Comput. Methods Programs Biomed.*, vol. 206, Jul. 2021, Art. no. 106121, doi: 10.1016/j.cmpb.2021.106121.

[26] X. Huang, J. Shan, and V. Vaidya, "Lung nodule detection in CT using 3D convolutional neural networks," in *Proc. IEEE 14th Int. Symp. Biomed. Imag. (ISBI)*, Apr. 2017, pp. 379–383.

[27] W. Zhu, C. Liu, W. Fan, and X. Xie, "DeepLung: Deep 3D dual path nets for automated pulmonary nodule detection and classification," in *Proc. IEEE Winter Conf. Appl. Comput. Vis. (WACV)*, Mar. 2018, pp. 673–681.

[28] A. Bhandary, G. A. Prabhu, V. Rajinikanth, K. P. Thanaraj, S. C. Satapathy, D. E. Robbins, C. Shasky, Y.-D. Zhang, J. M. R. S. Tavares, and N. S. M. Raja, ''Deep-learning framework to detect lung abnormality—A study with chest X-ray and lung CT scan images,'' *Pattern Recognit. Lett.*, vol. 129, pp. 271–278, Jan. 2020.
[29] E. Kim, K. H. Lee, and W. K. Sung, ''Recent trends in lightweight technology for deep neural networks,'' *Korean Inst. Inf. Sci. Eng.*, vol. 38, pp. 18–29, Aug. 2020.
[30] C. M. Kim, E. Hong, K. Chung, and R. Park, ''Line-segment feature analysis algorithm using input dimensionality reduction for handwritten text recognition,'' *Appl. Sci.*, vol. 10, no. 19, pp. 6904–6921, Oct. 2020.
[31] C.-M. Kim, K.-H. Kim, Y. S. Lee, K. Chung, and R. C. Park, ''Real-time streaming image based PP2LFA-CRNN model for facial sentiment analysis,'' *IEEE Access*, vol. 8, pp. 199586–199602, Oct. 2020.
[32] C. M. Kim, E. Hong, K. Chung, and R. Park, ''Driver facial expression analysis using LFA-CRNN-based feature extraction for health-risk decisions,'' *Appl. Sci.*, vol. 10, pp. 2956–2974, Apr. 2020.
[33] B. M. Maweu, S. Dakshit, R. Shamsuddin, and B. Prabhakaran, ''CEFEs: A CNN explainable framework for ECG signals,'' *Artif. Intell. Med.*, vol. 115, May 2021, Art. no. 102059, doi: 10.1016/j.artmed.2021.102059.
[34] I. Carrard, S. Rothen, and R. F. Rodgers, ''Body image concerns and intuitive eating in older women,'' *Appetite*, vol. 164, Sep. 2021, Art. no. 105275, doi: 10.1016/j.appet.2021.105275.
[35] *VUNO Med-Chest X-Ray System*. Accessed: Jan. 19, 2021. [Online]. Available: https://www.vuno.co/
[36] *Auto Lung Nodule Detection of Samsung Electronics*. Accessed: Jan. 19, 2021. [Online]. Available: https://samsunghealthcare.com/
[37] A. Brahim, R. Jennane, R. Riad, T. Janvier, L. Khedher, H. Toumi, and E. Lespessailles, ''A decision support tool for early detection of knee OsteoArthritis using X-ray imaging and machine learning: Data from the OsteoArthritis initiative,'' *Comput. Med. Imag. Graph.*, vol. 73, pp. 11–18, Apr. 2019.
[38] Y. Dong and S. J. Qin, ''A novel dynamic PCA algorithm for dynamic data modeling and process monitoring,'' *J. Process Control*, vol. 67, pp. 1–11, Jul. 2018.
[39] T. Ozturk, M. Talo, E. A. Yildirim, U. B. Baloglu, O. Yildirim, and U. R. Acharya, ''Automated detection of COVID-19 cases using deep neural networks with X-ray images,'' *Comput. Biol. Med.*, vol. 121, Jun. 2020, Art. no. 103792, doi: 10.1016/j.compbiomed.2020.103792.
[40] L. T. Phan, T. V. Nguyen, Q. C. Luong, T. V. Nguyen, H. T. Nguyen, H. Q. Le, T. T. Nguyen, T. M. Cao, and Q. D. Pham, ''Importation and human-to-human transmission of a novel coronavirus in vietnam,'' *New England J. Med.*, vol. 382, no. 9, pp. 872–874, Feb. 2020.
[41] L. Brunese, F. Mercaldo, A. Reginelli, and A. Santone, ''Explainable deep learning for pulmonary disease and coronavirus COVID-19 detection from X-rays,'' *Comput. Methods Programs Biomed.*, vol. 196, Nov. 2020, Art. no. 105608, doi: 10.1016/j.cmpb.2020.105608.

CHANG-MIN KIM received the B.S. and M.S. degrees from the Department of Computer Information Engineering, Sangji University, Wonju, South Korea, in 2014 and 2016, respectively, where he is currently pursuing the Ph.D. degree with the Department of Information Communication Software Engineering. His research interests include computer vision, database, artificial networks, programming language, data mining artificial intelligence, machine learning, and deep learning.

ELLEN J. HONG received the B.S. degree in electrical engineering from Pusan National University (PNU), Busan, in 2005, and the M.S. and Ph.D. degrees in electrical engineering from KAIST, Daejeon, in 2007 and 2013, respectively. From 2013 to 2016, she was a Postdoctoral Researcher with KAIST and PNU. From 2016 to 2017, she was a Professor with the Division of Computing Engineering, Dongseo University, Busan. From 2018 to 2019, she was a Research Engineer with the Convergence Laboratory, KT. Since 2019, she has been with Yonsei University, Wonju, where she is currently a Professor with the Division of Software. Her research interests include deep learning, digital twin, cyber physical systems, and evolutionary computation.

ROY C. PARK received the B.S. degree from the Department of Industry Engineering, Sangji University, Wonju, South Korea, and the M.S. and Ph.D. degrees from the Department of Computer Information Engineering, Sangji University, in 2010 and 2015, respectively. From 2015 to 2018, he was a Professor with the Division of Computing Engineering, Dongseo University, South Korea. Since 2019, he has been a Professor with the Department of Information Communication Software Engineering, Sangji University. His research interests include WLAN systems, heterogeneous networks, ubiquitous network services, human-inspired artificial intelligent and computing, health informatics, knowledge systems, peer-to-peer, and cloud networks.